Superconductor Science and Technology

PAPER

Analysis of ITER NbTi and Nb_3Sn CICCs experimental minimum quench energy with JackPot, MCM and THEA models

To cite this article: T Bagni *et al* 2017 *Supercond. Sci. Technol.* **30** 095003

IOP Publishing Superconductor Science and Technology
Supercond. Sci. Technol. **30** (2017) 095003 (10pp) https://doi.org/10.1088/1361-6668/aa7a80

Analysis of ITER NbTi and Nb_3Sn CICCs experimental minimum quench energy with JackPot, MCM and THEA models

T Bagni[1,2], J L Duchateau[3], M Breschi[4], A Devred[3] and A Nijhuis[1]

[1] University of Twente, Faculty of Science & Technology, 7522 NB Enschede, The Netherlands
[2] Ghent University, Department of Applied Physics, B-9000 Gent, Belgium
[3] ITER Organization, Route de Vinon-sur-Verdon, F-13067, St Paul Lez Durance Cedex, France
[4] Universitá di Bologna, Dipartimento di Ingegneria dell'Energia Elettrica e dell'Informazione 'Guglielmo Marconi', Viale Risorgimento, Bologna, Italy

E-mail: t.bagni@utwente.nl

Received 5 April 2017, revised 1 June 2017
Accepted for publication 20 June 2017
Published 26 July 2017

Abstract

Cable-in-conduit conductors (CICCs) for ITER magnets are subjected to fast changing magnetic fields during the plasma-operating scenario. In order to anticipate the limitations of conductors under the foreseen operating conditions, it is essential to have a better understanding of the stability margin of magnets. In the last decade ITER has launched a campaign for characterization of several types of NbTi and Nb_3Sn CICCs comprising quench tests with a singular sine wave fast magnetic field pulse and relatively small amplitude. The stability tests, performed in the SULTAN facility, were reproduced and analyzed using two codes: JackPot-AC/DC, an electromagnetic-thermal numerical model for CICCs, developed at the University of Twente (van Lanen and Nijhuis 2010 *Cryogenics* **50** 139–148) and multi-constant-model (MCM) (Turck and Zani 2010 *Cryogenics* **50** 443–9), an analytical model for CICCs coupling losses. The outputs of both codes were combined with thermal, hydraulic and electric analysis of superconducting cables to predict the minimum quench energy (MQE) (Bottura *et al* 2000 *Cryogenics* **40** 617–26). The experimental AC loss results were used to calibrate the JackPot and MCM models and to reproduce the energy deposited in the cable during an MQE test. The agreement between experiments and models confirm a good comprehension of the various CICCs thermal and electromagnetic phenomena. The differences between the analytical MCM and numerical JackPot approaches are discussed. The results provide a good basis for further investigation of CICC stability under plasma scenario conditions using magnetic field pulses with lower ramp rate and higher amplitude.

Keywords: cable-in-conduit conductors, fusion magnets, stability, ITER, quench model

(Some figures may appear in colour only in the online journal)

Introduction

The ITER Organization has experimentally characterized several NbTi and Nb_3Sn CICCs in the SULTAN facility. The tests include AC loss for all cables and MQE measurements for most of the NbTi conductors and only few central solenoid (CS) conductors. The AC losses are generated at different frequencies of a sinusoidal transversal applied magnetic field and the energy deposited is determined using calorimetry [4]. The MQE tests are performed using a truncated single sine wave magnetic field pulse. The fast variations generate current loops and heat dissipation, which causes a quench when exceeding a critical level of energy.

In a superconducting composite strand, the transverse currents between the filaments generate AC coupling loss. An applied external transverse magnetic changing field with amplitude B_a, creates a reacting field inside the strand of value $\tau(dB_i/dt)$ [5]. In this condition, the power loss generated by

the transverse currents is deposited inside the strand volume and can be expressed by the equation:

$$P = \frac{2\tau\left(\frac{dB_i}{dt}\right)^2}{\mu_0}. \quad (1)$$

The structure of a CICC is significantly different from that of a strand. The use of a global time constant τ to represent the AC coupling loss of a multistage cable can be convenient and accurate for gradual variations of magnetic field (dB/dt), but this approximation fails to describe the behavior in faster field variations. With the same methodology, the coupling loss can be fitted analytically assuming the presence of several time constants associated to volume fractions in the CICC [6, 7]. The MCM model uses some simplifications by adopting the concept of several stages, each represented by a time constant τ_i, with the aim of modeling the interactions between the stages. The parameters of the MCM are calculated, for a given ITER conductor, by fitting the experimental ac losses tests in Sultan in a given range of frequency, typically 0.1–5 Hz [8].

A different method to model CICCs coupling losses is using a numerical approach. The code JackPot-AC/DC is able to model a complete CICC as a network of superconducting and resistive elements. Its backbone is the cabling subroutine that calculates the trajectories of all the strands inside the cable. All involved model parameters are obtained from geometrical dimensions and experiments, thus there are no free parameters in the model. Starting from the cable design, JackPot generates a complete CICC geometry, with strand level detail, using experimentally determined properties of the strands with mutual inductive coupling between strands and coupling with the applied magnetic field. The numerical code is able to calculate critical current and current distribution in all individual strands, at any location in the cable and for any chosen scenario. Based on the local power and heat generation, AC loss and stability can be evaluated in a chosen scenario. After the proper calibration finding the inter-strand contact resistivity, it is possible to successfully calculate the energy deposited inside the cable during the MQE tests and to look into the details of the electromagnetic performance of the CICC, such as current distribution and peak electric fields at strand level.

In this study, the THEA code (CryoSoft [9]) is used in combination with MCM and JackPot respectively, to model the thermal behavior of two samples during their MQE tests. One conductor from the ITER Poloidal Field coil #1 called PFEU2 [10] and one ITER CS conductor, the CSJA8 sample [11]. The aim is to evaluate the agreement between THEA calculations and the recent stability experiments in view of a possible prediction of the margin with a different disturbance profile relevant for the ITER plasma-operating scenario.

In figure 1 the content of the paper is shown schematically. We compare the use of MCM and JackPot-AC/DC, both in combination with THEA for the analysis of the NbTi and Nb_3Sn conductors. JackPot-AC/DC is able to simulate the behavior of a conductor under every coil operating scenario condition since it has incorporated a very detailed description of the conductor geometry, transport and coupling currents in all strands [12, 13]. This way it is able to handle all transport current, self-field and applied field variations in time and extrapolative predictions are well possible. For the analytical MCM, the modeling options seem more constrained since the approach is based on sinusoidal applied magnetic fields without transport current and wire bundles are represented by single coupling loss time constants. Using THEA and JackPot-AC/DC should allow to have a complete view of the thermal and electromagnetic behavior of a CICC during fast magnetic field transients of any evolution in time.

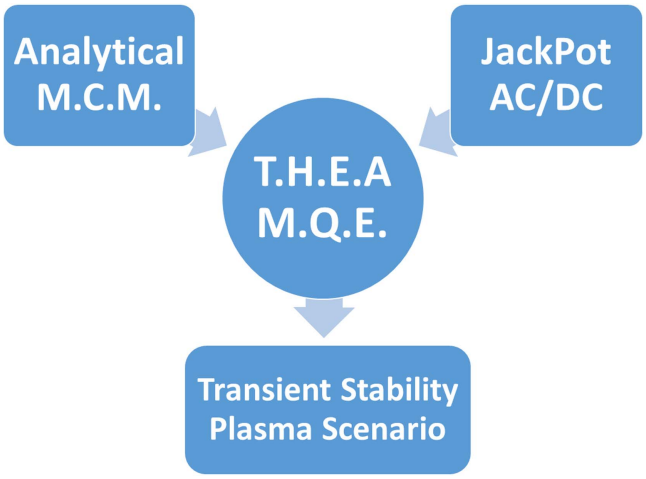

Figure 1. Overall scheme of the present study. Both MCM and JackPot-AC/DC will be used in combination with THEA to model the SULTAN stability tests in order to extrapolate towards the ITER plasma scenario performance.

MQE test and analysis

Sample preparation

The SULTAN NbTi sample is made from one conductor unit length bent in a hairpin U-shape [14], while the Nb_3Sn sample is made of two conductor sections of the same length joined at the ends obtaining a U-shape configuration [15]. The central channel of the conductor is blocked, thus the helium can flow only in the bundle with a mass flow rate from 1 to 10 g s^{-1}. In the SULTAN facility the sample is vertically inserted in the magnet bore [16] and the upper terminations are electrically connected to the current leads of the superconducting transformer. The magnet system generates both DC and AC fields, orthogonal oriented to each other. The DC high field zone (HFZ) is ~450 mm long while the AC field has an effective length of ~390 mm. The AC coil can generate a continuous or singular sinusoidal variable magnetic field on the conductor to induce AC loss and consequently a quench during MQE tests. The instrumentation used during the tests was optimized for the qualification of the ITER samples [17]. The sample voltage taps and temperature sensors are located upstream and downstream the HFZ. The measured energy for AC loss and MQE is normalized using the superconducting composite volume (V) exposed to the AC magnetic field.

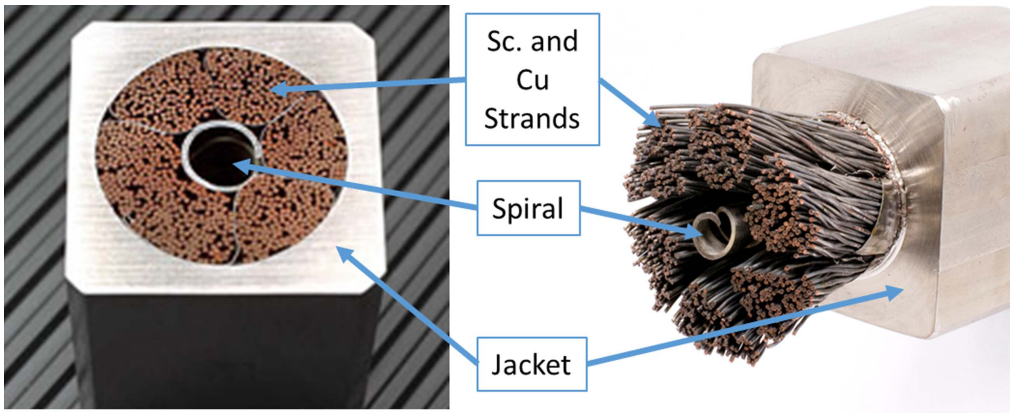

Figure 2. Cross section of a NbTi poloidal field coil (left) and a Nb_3Sn central solenoid (right) conductors (Courtesy of C Sanabria, formerly FSU, © CC BY 4.0).

MQE test and analysis

The MQE tests aim as a basic input to study the stability of ITER conductors under various operating conditions. The tests are carried out in the presence of a background field and with transport current. The energy in the conductor is injected applying a fast singular sinusoidal pulsed field using the AC coil that induces eddy current and coupling losses in the sample. This amplitude of the applied sinusoidal single pulse is increased stepwise progressively until a quench occurs. The MQE assessment procedure is detailed in [18]. The energy deposited is determined considering the helium temperature difference, measured between upstream and downstream sensors and by using the mass-flow rate and the helium specific heat [19]. The error bars involved in the energy extrapolation are unpredictable, due to the fluctuation in the helium temperature. Especially for the Nb_3Sn conductor because the higher the initial temperature, the more unstable the thermometer measurements are. The error in the temperature difference is minimized considering the helium shift between upstream and downstream sensors related with the helium velocity.

The samples analyzed in this study are the PFEU2 NbTi conductor and the CSJA8 Nb_3Sn conductor. Only one leg of the sample is considered for analysis because a quench is generated only in one leg. Both legs are not perfectly similar and the difference causes one leg to quench before the other.

The main parameters of the conductor are summarized in table 1, figure 2 shows the cross section of poloidal field and CS conductors.

A typical plot of a MQE test is shown in figure 3. The energy per unit of volume deposited during the fast singular pulsed field transition is plotted as a function of the pulsed field maximum amplitude. The energy that determines a quench is not directly measurable, because the self-heating generated from the quench increases dramatically the temperature obscuring completely the heat deposition due to the magnetic field pulse. Therefore, the quench energy (yellow mark) is extrapolated by a linear fit from the previous values of energy with lower magnetic field pulse amplitude (B_a). The figure shows the impact of the operating temperature on the MQE at a transport current of 44 kA. The higher the operating temperature is, the lower is the deposited energy and consequently the magnitude of the magnetic field pulse necessary to initiate a quench.

MQE modeling

The stability tests, performed in the SULTAN facility, were reproduced and analyzed using two codes: JackPot-AC/DC and MCM, both coupled with THEA.

THEA model

The THEA code is a 1D model, used to analyze the superconducting thermal and hydraulic behavior of the conductor. The conductor is defined using thermal and hydraulic elements. Superconducting strands, copper strands and jacket represent the thermal elements, listed in table 1. The hydraulic elements are the coolant parameters, like helium mass-flow, cross-sectional area of the bundle, A, wetted perimeter, Wp, void fraction as listed in table 2.

Both PFEU2 and CSJA8 are modeled using a simplified design composed of a 1.5 m long conductor, divided in two thermal elements. The first element is the superconductor and copper composite modeled like a single component instead of hundreds of strands and the second element is the stainless steel jacket. The superconductor and the resistive stabilizer are assumed to be electrically and thermally in parallel. The hydraulic part is the supercritical helium flowing in the bundle. The helium in the central channel is not taken into account because in the SULTAN sample the channel is closed to force the coolant to flow only in the bundle. However, few simulations including the central channel were made to study its influence on stability during fast heat depositions ($<$150 ms). The result shows that there is no influence on the stability coming from the presence of the central channel under such conditions.

The current sharing temperature, T_{cs}, of the CICCs is measured in SULTAN, using the electric field threshold of $E_c = 10\ \mu V\ m^{-1}$, and modeled using the ITER scaling laws for

Table 1. Parameters of the ITER conductors.

	PFUE2	CSJA8
Shape	Circle-in-square	Circle-in-square
Main outer dimension (mm)	53.8 × 53.8	49.0 × 49.0
Target jacket inner diameter (mm)	37.7	32.6
Target central spiral diameter (mm)	10–12	7–9
Cable layout	3sc × 4 × 4 × 5 × 6	(2sc + 1Cu) × 3 × 4 × 4 × 6
Jacket material	3161	JK2LB
Void fraction (%)	34.3	33.6
Joint layout	Hairpin	Solder filling
Strand	ChMP	KAT
Strand Cu:nonCu	1.59	1
RRR	>100	>100
A supercond. (mm^2)	229	322
A copper (mm^2)	366	322
A bundle ($mm^{2)}$)	595	482
A jacket ($mm^{2)}$)	1432	1566

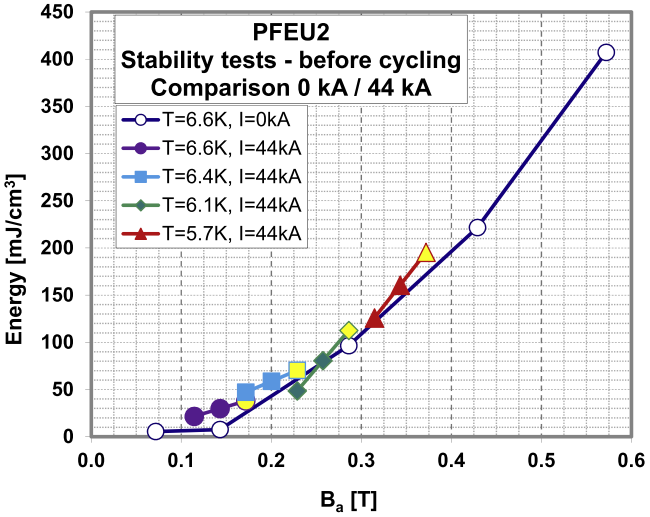

Figure 3. Experimental MQE test results of the PFEU2 sample before the EM cyclic loading. The value B_a represents the peak magnetic field applied on the conductor during the stability test to generate the quench. The yellow symbol is the estimated energy that initiates a quench in the conductor at each operating temperature.

Table 2. Hydraulic data for the THEA model.

	PFUE2	CSJA8
A_{Helium} (mm^2)	344	259
Wp_{bundle} (mm)	3667	2558
Wp_{jacket} (mm)	118	103
Void fraction (%)	34.3	33.6
Mass flow ($g\,s^{-1}$)	2.5	3.3

NbTi [20] and Nb_3Sn [21] with the parameters defined in [10, 11]. The boundary conditions, applied in the model (background field and transport current), are the same as used during the experiments, see table 3.

To reproduce the MQE test in THEA, only a thermal load is applied to the conductor. In THEA the energy is directly injected in the composite as heating power while the magnetic field applied is considered constant during the simulation, see table 3 [22]. This approximation is allowed because the AC and DC fields are orthogonal and B_{dc} is five to ten times larger than B_a. Therefore the T_{cs} and I_c are only weakly influenced by the fast transient field. The peak magnetic field applied on the conductor can be easily calculated as background field plus the self-field generated by the operation current in the two conductors, using the simple equation:

$$B_{peak} = B_{dc} + \frac{\mu_0 I_{op}}{2\pi} \cdot \left(\frac{1}{r} + \frac{1}{a-r}\right), \qquad (2)$$

where B_{dc} is the background field, I_{op} is the operation current, μ_0 the magnetic permeability in the vacuum, r is the conductor radius and a is the distance between the leg centers [18].

In the THEA model, the MQE is calculated following the same procedure as in the SULTAN experiment. The energy is injected by using a truncated sinusoidal pulse with stepwise increase of the amplitude until a quench occurs. The last energy value injected before the quench initiation is defined as MQE. Therefore, instead of the usual constant power pulse that is mostly used in THEA simulations, the heat deposition profile is modeled now with a truncated sinusoidal profile for which we can use the MCM and JackPot-AC/DC models.

Table 3. PFEU2 and CSJA8 MQE boundary conditions.

	PFUE2	CSJA8
Peak field (T)	5.2	9.6
Background field (B_{dc}) (T)	4.5	9.0
Current (kA)	44	40
Temperatures (K)	5.7–6.6	7.7–8.6
Pulse duration (ms)	128	128
Pulse amplitude (B_a) (T)	0.1–0.35	0.3–0.5

MCM analytical model

The MCM is calibrated by fitting the SULTAN AC loss measurements using a set of multiple time constant τ and volume fraction k, one for every cabling stage, as presented in [2]. The expression used to calculate the power dissipated in the CICC is derived from equation (1), where $B_{ext}(t) = B_a \sin(\omega t)$ is the sinusoidal external applied magnetic field and B_{int} is the magnetic field inside the conductor, expressed as [8]:

$$B_{int} = \frac{B_a}{\sqrt{\omega^2\tau^2+1}} \sin(\omega t - \delta). \quad (3)$$

In (3) B_a is the pulse amplitude, t_0 is the pulse period (128 ms), ω the angular velocity, τ the time constant, $\delta = \arctan(\omega\tau)$.

For the power calculation, we use the dB_{int}/dt in equation (1):

$$\text{where } dB_{int}/dt \text{ is: } \dot{B}_{int} = \frac{B_a\omega}{\sqrt{\omega^2\tau^2+1}} \cos(\omega t - \delta). \quad (4)$$

For the MQE tests, the single magnetic field pulse is not represented by a perfect sine wave but the fast transient generated by the SULTAN coil is a truncated sinusoid. This shape can be analytically expressed by a pseudo sinusoidal equation defined as follows:

$$B_{intI} = \frac{B_a}{\sqrt{\omega^2\tau^2+1}}[\sin(\delta)e^{\left(-\frac{t}{\tau}\right)} + \sin(\omega t - \delta)] \quad \text{for } 0 < t < t_0, \quad (5)$$

$$B_{intII} = \frac{B_a}{\sqrt{\omega^2\tau^2+1}} \sin(\delta)(1 - e^{-\frac{t_0}{\tau}})e^{-\frac{t}{\tau}} \text{ for } t > t_0. \quad (6)$$

Then starting from (5) and (6) we can define:

$$\dot{B}_{intI} = \left\{\frac{B_a}{\sqrt{\omega^2\tau^2+1}}\left[\omega\cos(\omega t - \delta) - \frac{1}{\tau}\sin(\delta)e^{\left(-\frac{t}{\tau}\right)}\right]\right\} \quad \text{for } 0 < t < t_0, \quad (7)$$

$$\dot{B}_{intII} = \left\{-\frac{B_a}{\tau}\frac{1}{\sqrt{\omega^2\tau^2+1}} \sin(\delta)(1 - e^{-\frac{t_0}{\tau}})e^{-\frac{t}{\tau}}\right\} \quad \text{for } t > t_0. \quad (8)$$

With equations (7) and (8), we can define the power deposited during the MQE test as:

$$P = \sum_n \frac{k_n \tau_n \dot{B}^2_{int_n}(t)}{\mu_0}, \quad (9)$$

where n is the number of time constants chosen to model the conductor. In figure 4 the comparison between a perfect sine wave and the truncated sinusoid generated by the equations above is shown.

MCM-THEA simulations

An example of the THEA output computed with MCM is shown in figure 5 where the PFEU2 is modeled during a MQE test with 128 ms duration of the heat deposition

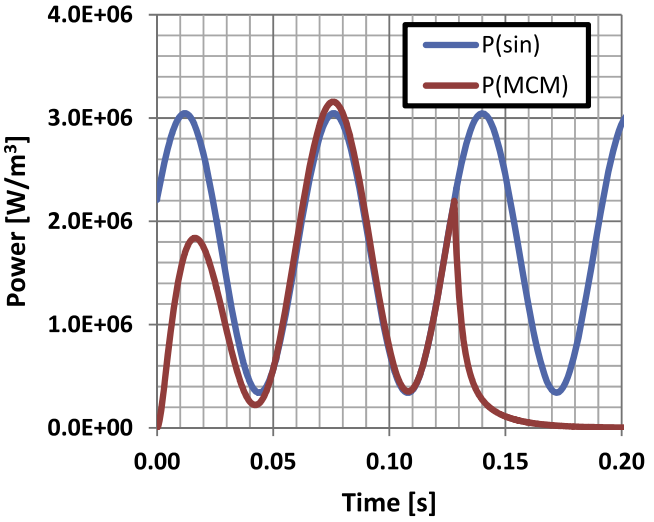

Figure 4. Compared power profiles for the permanent and the truncated sinusoid corresponding to the MCM (T_0 = 128 ms, B_a = 0.2 T).

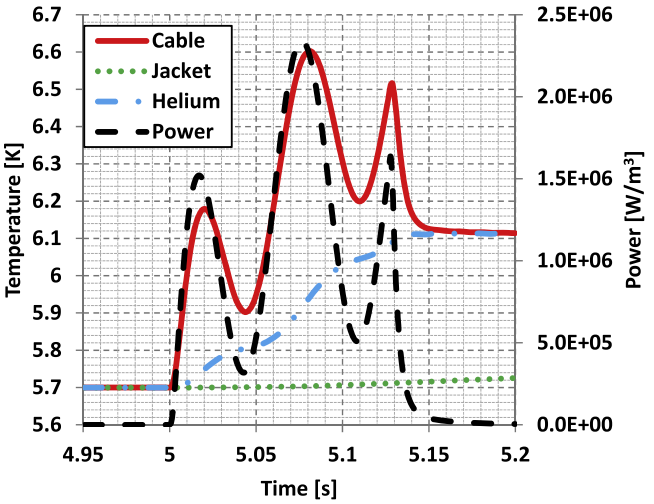

Figure 5. Example of a THEA simulation of the PFEU2 sample calculated with the MCM model. The injected power (black line, right ordinate) is based on the truncated sinusoidal magnetic field pulse. The calculated temperature variation of cable, jacket and helium are shown during the heat deposition (left ordinate).

generated by the single sinusoidal magnetic field pulse. The increase of the cable temperature is faster than the helium heat removal, therefore the cable is able to reach and exceed the T_{cs}, even if the helium temperature is still lower. In the example, the cable reaches 6.6 K, while the helium is still at 6.0 K.

The MCM is calibrated by fitting the SULTAN AC loss measurements that are different in terms of temperature and applied magnetic field amplitude from those used during the MQE stability tests. These differences can have an impact on the power calculation since the temperature affects the critical current possibly creating saturation. In figures 6 and 7, the energy calculated with MCM using the SULTAN MQE magnetic field amplitude, B_a, is compared with the energy extracted from the experimental stability tests. The open dots

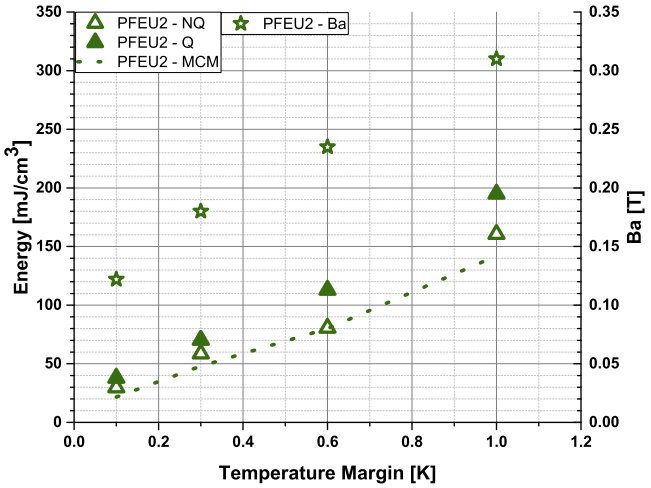

Figure 6. PFEU2—on the left axes, the energy measured in SULTAN during the stability tests, open dots represent recovery while full dots indicate quench. The dashed line is the energy calculated using MCM. On the right axes, the magnetic field amplitude B_a used during the stability test.

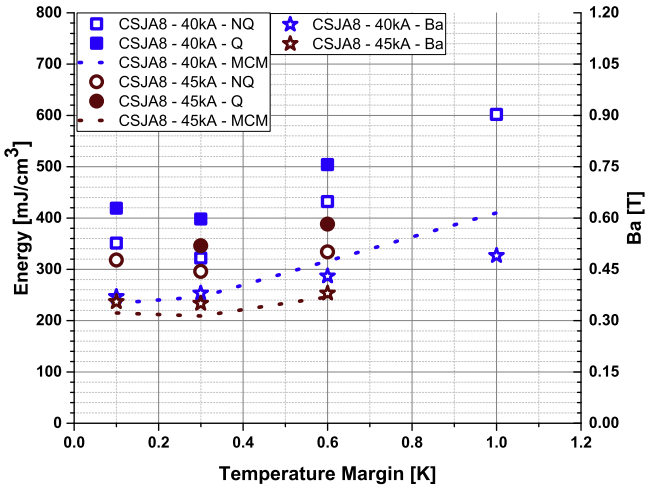

Figure 7. CSJA8—on the left axes, the energy measured in SULTAN during the stability tests, open dots represent recovery while full dots indicate quench. The dashed lines are the energy calculated using MCM. On the right axes, the magnetic field amplitude B_a used during the stability test.

represent recovery, while full dots indicate a quench of the sample in all following plots; the actual MQE is between these limits. The dashed lines are the energy calculated by using MCM. The magnetic field amplitude Ba used during the stability test is plotted as well, scaled on the right axes.

The results of the PFEU2 show a good match between MCM and experiment, while for CSJA8 the MCM calculated energy is significantly below measured values, about 100–200 mJ cm^{-3} (35%) lower than SULTAN MQE. This discrepancy in the MCM results is likely due to the fact that extrapolative scaling by using the MCM analytical expressions leads to an unpredictable error.

The energy discrepancy found for the Nb_3Sn sample by the MCM analytical equation is scaled by a correction factor in order to match the experimental energy values. The scaled

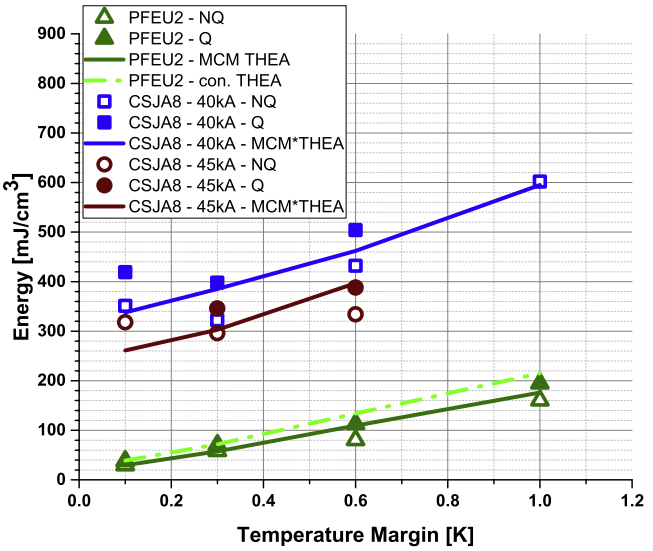

Figure 8. Minimum quench energy of PFEU2 and CSJA8 conductors as a function of the temperature margin between the T_{cs} and the operating temperature during the test. All the results in this plot have been obtained with the conductor boundary conditions listed in table 3. The lines represent the MQEs calculated with MCM-THEA (solid line) and constant (dashed line) energy deposition, the points are the experimental data coming from the SULTAN tests. Open dots indicate recovery, full dots represent a quench.

value is then used in THEA to model the power dissipation in time with the truncated sinusoidal profile. These results are indicated in the following as MCM*.

In figure 8 the MQE from the MCM-THEA simulations for the PFEU2 and CSJA8 samples at different temperature margin and tweaked for the quantitative energy output are compared with the experimental MQE tests.

The temperature margin is the difference between the T_{cs} and the operating temperature. All the results in the plot have been obtained with the conductor boundary conditions listed in table 3. The solid lines represent the MQEs calculated with MCM-THEA while the markers are the experimental data coming from the SULTAN tests.

In order to understand the effect of the applied perturbation time-profile on the MQE, instead of using the MCM profile in the PFEU2 model, the energy was injected using constant heat deposition in time. In that case, the model predicts a higher level of MQE, see figure 8. By changing the profile of the heating deposition, the MQE is modified by ~20%. This means that the THEA results are as accurate as the expression of the perturbation in the conductor. To have a correct representation of the MQE, it is evidently necessary to accurately evaluate the perturbation profile. The dashed line is calculated for constant energy deposition with pulse duration of 128 ms.

The THEA model, with MCM input (adjusted for Nb_3Sn), shows good agreement with the SULTAN MQE tests even if it is a simplification of the real CICC layout. The simulated MQE is mostly in between the no-quench and quench measured limits.

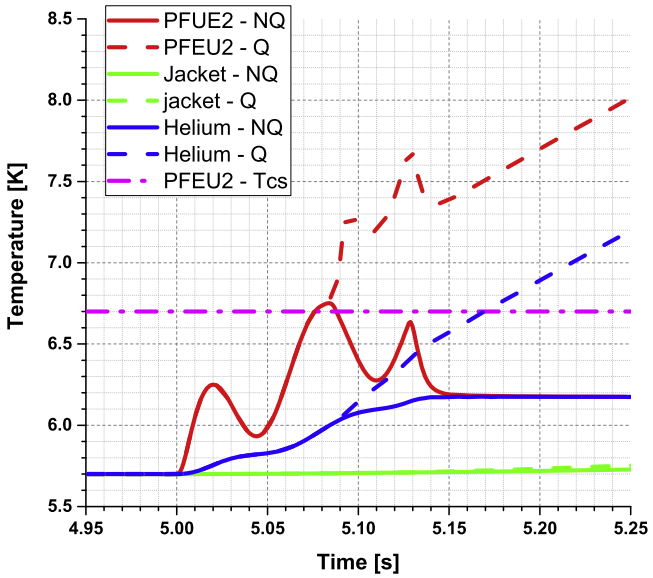

Figure 9. PFEU2 temperature profile calculated by MCM-THEA. The solid lines represent the temperature fluctuation during the MQE simulation for the cable and the helium, while the dashed lines represent the temperature evolution during a quench. The horizontal dashed line represents the measured T_{cs} of the PFEU2 cable. The simulation boundary conditions are $B_{dc} = 4.5$ T, $I_{op} = 44$ kA, $T_{in} = 5.7$ K.

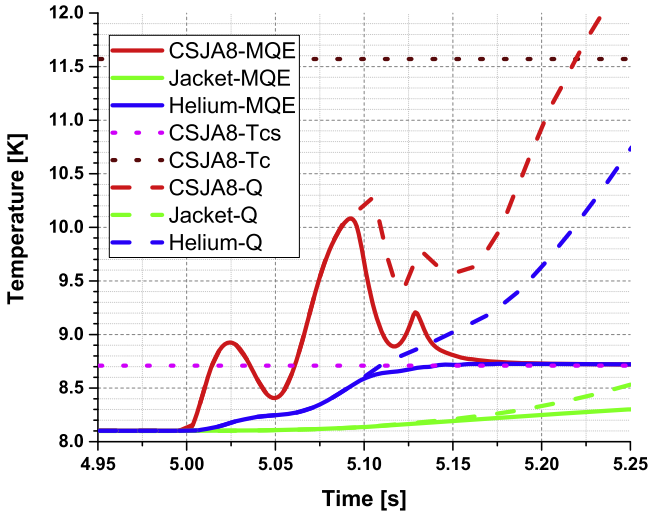

Figure 10. CSJA8 temperature profile calculated by MCM*-THEA, the solid lines represent the temperature fluctuation during the MQE simulation for the cable and the helium, while the dashed lines represent the temperature evolution during a quench. The horizontal dashed lines represent the measured T_{cs} and the calculated T_c of the CSJA8 cable. The simulation boundary conditions are $B_{dc} = 9$ T, $I_{op} = 40$ kA, $T_{in} = 8.1$ K.

Following the temperature evolution of conductor and coolant it is possible to determine the start of the quench, see figures 9 and 10. The energy is injected in the conductor using the truncated sinusoidal pulse and the maximum power is reached in the central peak (see figure 5), which corresponds in this case to the maximum cable temperature. The results show that the central peak temperature, which is the most severe, triggers the quench. It also appears that if the conductor is able to survive the central peak, the power deposition from the third peak is not able to trigger a quench.

When a NbTi conductor exceeds the T_{cs} by a few mK, part of the NbTi changes from superconducting to normal state and the helium is not capable to recover the superconductivity. Accordingly, as a result of an avalanche like process, the whole cable quenches. However, the Nb_3Sn conductor is still able to recover far above its T_{cs} (~8.7 K), even reaching 10.1 K before initiating a quench. This difference between NbTi and Nb_3Sn can be explained by the definition of the current sharing temperature and the steepness of the transition from superconductive to normal state [23]. The T_{cs} is the temperature associated with a defined critical electric field $E_c = 10\ \mu V\ m^{-1}$ [24]. The local electric field is expressed as:

$$E = E_c\left(\frac{I_{strand}}{I_c}\right)^n, \tag{10}$$

where I_c is critical current, I_{strand} is current flowing in the strand and n defines the steepness of the transition, which is ~30 for NbTi and ~5 for the ITER Nb_3Sn CICC conductors. The smaller value of n allows Nb_3Sn to have a much smoother transition and to recover even from temperatures significantly exceeding T_{cs}. Opposite result was found for NbTi and Nb_3Sn single strand comparison, where a NbTi strand was able to recover even after crossing T_{cs}, while a Nb_3Sn strand was not [25]. The Nb_3Sn behavior was explained by the low conductivity of the bronze matrix but probably also the different n-value, compared with the CSJA8 CICC, could be playing a role.

JackPot-AC/DC model

JackPot-AC/DC models a full CICC as a network of superconducting and resistive elements describing the trajectories of all the strands inside the cable without any free parameters in the model except one; the value of the inter-strand contact resistivity (R_{ss}) [1]. The contact area between strands in contact with each other determines the distribution of the inter-strand contact resistance and this is determined by the cable pattern. The strand elements are mutually inductively coupled with each other and with the applied magnetic field. The parameters used for the conductor and the strands scaling law are the same as used for the THEA model listed in table 1 and in [10]. During the SULTAN tests, the combination of magnetic field and transport current causes Lorentz forces in the conductor that influence the inter-strand and inter-petal resistivity. JackPot is able to account for the mechanical effect of the Lorentz force on the cable by fitting the contact resistivity values used in the simulations to the PFEU2 and CSJA8 AC loss measurements with and without transport current [12]. The hysteretic loss is subtracted from the total AC loss in order to compare only the coupling loss contribution. Figure 11 shows the measured and calculated coupling loss of the CSJA8 sample. The resistivity parameters obtained from the fit were used for the MQE simulations since AC loss and MQE experiments have similar boundary conditions regarding background field and transported current. The

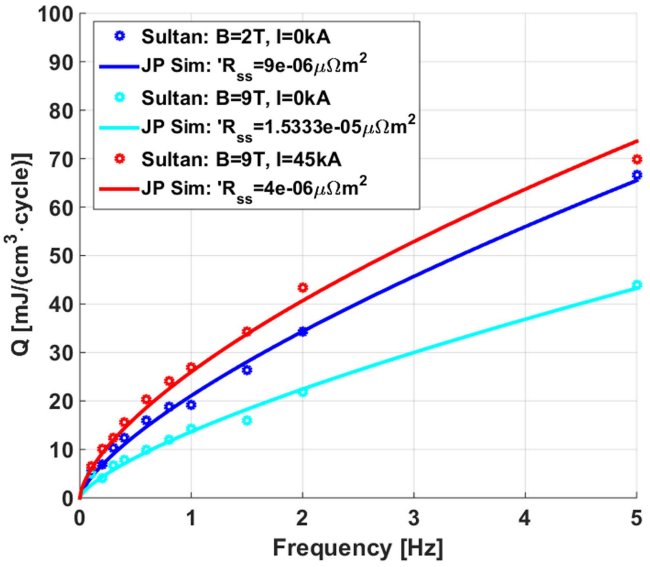

Figure 11. CSJA8 measured and calculated coupling current loss at $B_a = 0.2$ T. The dots represent SULTAN measurements while the lines are the JackPot simulations.

simulated cable length corresponds to the AC coil length, it is the region were most of the coupling losses are generated, the interaction with the sample joint is neglected, while the second leg is considered incrementing the magnetic field, see table 3.

JackPot-THEA simulations

After the calibration of the inter-strand contact resistance, the MQE tests can be simulated by the JackPot-THEA combination. The output power calculated by JackPot is used as input in THEA, instead of using the analytical MCM equation. The temperature, background magnetic field and transport current are set to the same values in JackPot as used in the table 3. The sinusoidal magnetic field pulse used in JackPot has the same amplitude and shape as the pulsed field used in the SULTAN stability experiment.

The power versus time deposited during a MQE test computed with JackPot is shown in figure 12, and compared to the MCM* result for the CSJA8 sample. Although there is a difference between both model results, the profile generated with the MCM* code resembles closely the results of the more detailed JackPot approach.

The JackPot routines are not extended for simulation of the quench initiation and propagation like in THEA, therefore it does not deliver the immediate MQE. However, JackPot is able to calculate precisely the instantaneous power generated during a magnetic field pulse in time and the linked complex current distribution inside the cable.

As for MCM, the JackPot coupling current losses, induced from the pulsed magnetic field inside the conductor, are compared with the energy deposited during the experiment, illustrating that the discrepancy between the measured and simulated MQE is less than ~10% for both the NbTi and Nb_3Sn sample, see figure 13. The energy measured in SULTAN is well in agreement with the energy calculated by

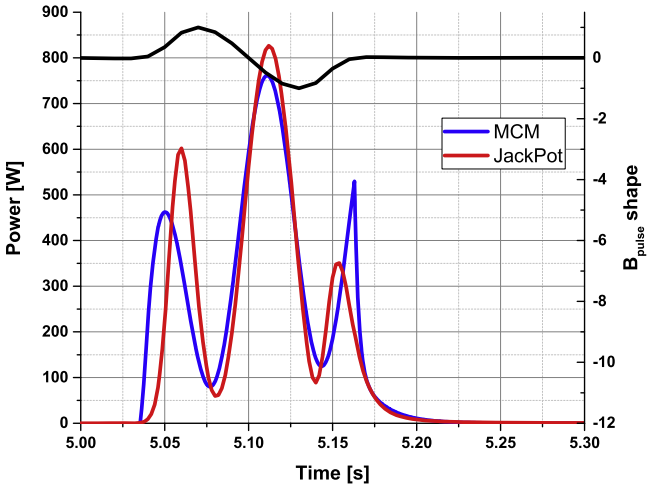

Figure 12. CSJA8 power versus time deposited during the MQE test at 0.3 K temperature margin. The red line is the power calculated by JackPot, while the blue line is the corrected power computed by MCM*. The black trace is the magnetic field pulse profile.

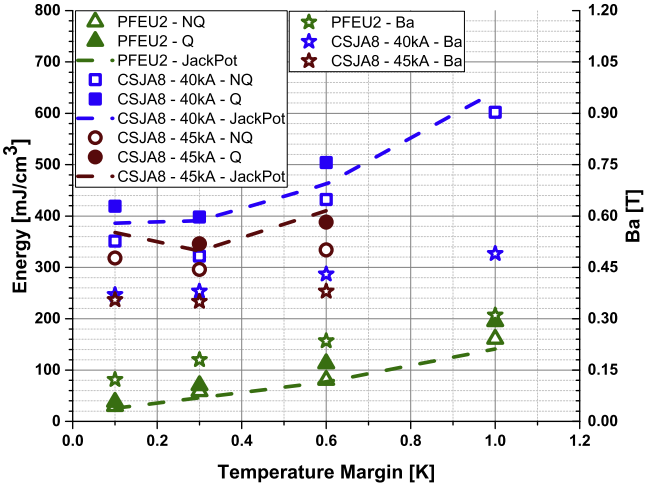

Figure 13. Left axes: MQE of CSJA8 and PFEU2 conductors computed by JackPot as a function of the temperature margin. The markers represent the experimental data from the SULTAN test (open dots indicate recovery, full dots quench) and the dashed lines are the JackPot simulations of the SULTAN test in recovery conditions. Right axes: the experimental magnetic field pulse amplitude, B_a, used for JackPor MQE calculation.

JackPot. After the validation of the JackPot energy calculation the combination JackPot and THEA is then used to calculate the MQE as function of the temperature margin.

Finding the MQE with JackPot+THEA is far more time demanding than using MCM-THEA because it is necessary to run a JackPot simulation for every magnetic field pulse and every temperature margin. Therefore, only one of the tested samples was reproduced with JackPot+THEA. After already finding the good agreement between PFEU2 and MCM it was more interesting to study the Nb_3Sn conductor. The test at 40 kA was selected because of the larger temperature margin interval, 0.1–1.0 K. As in the real experiment, the energy in the conductor is generated applying the fast singular sinusoidal pulsed field inducing the coupling losses in the sample.

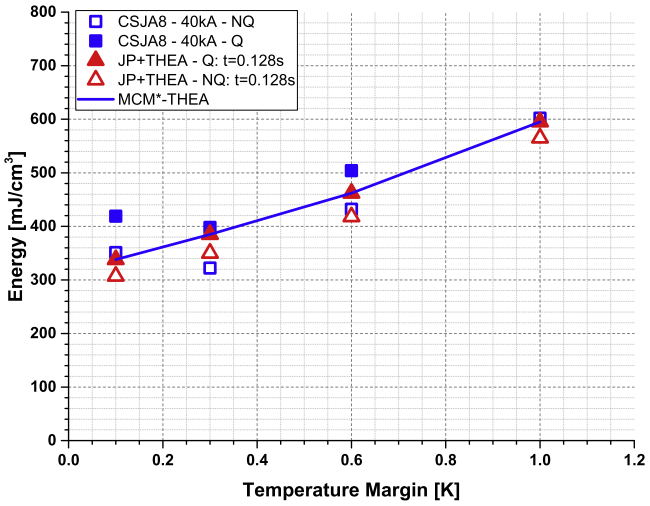

Figure 14. Minimum quench energy of CSJA8 conductor as a function of the temperature margin. The square markers represent the experimental data from the SULTAN tests, the red triangles are the JackPot+THEA simulation results. The open dots indicate recovery, full dots represent a quench. The line reflects the MQE calculated with the MCM*-THEA.

The pulse is applied by stepwise increasing the amplitude progressively until a quench occurs.

The JackPot+THEA computation results are shown in figure 14. The red triangles with open dots represent the energy calculated when the sample is still recovering, quenching for the filled dots. The combination of both models is able to well reproduce the experimental results in the entire range of temperature margin.

Conclusion

The power dissipation profile has a relevant impact on the cable stability, a constant heat deposition, rather than a truncated sinusoid deposition profile, can lead to significantly different quench energy threshold. Further investigation on different dissipation-time profiles is necessary to increase the comprehension for PS predictions.

The Nb_3Sn conductor, contrarily from the NbTi sample, is able to recover from the power deposition even if the temperature crosses T_{cs}; the difference in n-value is probably essentially responsible for this phenomena.

The MCM and JackPot models were compared after combining them with the THEA model for computation of the MQE. For the MCM-THEA models combination, it appears that MCM is not capable to predict precisely the amount of power generated during a time varying magnetic field pulse for the Nb_3Sn CICC. Therefore the MCM-THEA combination is not capable to predict the MQE starting only from magnetic field perturbation, temperature and current boundary conditions applied to the cable.

The JackPot model is able to calculate accurately the energy deposited inside a cable for any, time dependent, applied magnetic field, current and temperature. However, it is not adapted to compute the evolution of the quench propagation, although it can give the instant in time of reaching T_{cs}. Thus JackPot as stand-alone is capable to estimate the MQE of NbTi CICC conductors, because the quench transition occurs immediately when reaching T_{cs}. Nb_3Sn CICCs, on the other hands, are able to reach temperatures far above T_{cs} before quenching, therefore JackPot alone is not able to predict their exact MQE. Nonetheless, the combination JackPot+THEA is able to predict the SULTAN MQE experiment for CSJA8 with excellent agreement. This implies that JackPot+THEA provides a good basis for stability analyses of ITER coils subjected to severe alternating magnetic fields like the plasma-operating scenario.

Disclaimer

The views and opinions expressed herein do not necessarily reflect those of the ITER Organization.

ORCID

M Breschi https://orcid.org/0000-0001-9025-2487

References

[1] van Lanen E P and Nijhuis A 2010 JackPot: a novel model to study the influence of current non-uniformity and cabling patterns in cable-in-conduit conductor *Cryogenics* **50** 139–48
[2] Turck B and Zani L 2010 A macroscopic model for coupling current losses in cables made of multistages of superconducting strands and its experimental validation *Cryogenics* **50** 443–9
[3] Bottura L, Rosso C and Breschi M 2000 A general model for thermal, hydraulic and electric analysis of superconducting cables *Cryogenics* **40** 617–26
[4] Bruzzone P, Stepanov B, Wesche R, Ilyn Y, Herzog R, Calvi M, Bagnasco M and Cau F 2009 Methods, accuracy and reliability of ITER conductor tests in SULTAN *IEEE Trans. Appl. Supercond.* **19** 1508–11
[5] Campbell A M 1982 A general treatment of losses in multifilamentary superconductors *Cryogenics* **22** 3–16
[6] Nijhuis A, ten Kate H H, Duchateau J and Bruzzone P 1997 Coupling loss time constants in full-size Nb3Sn CIC model conductors for fusion magnets *Adv. Cryog. Eng. Mater.* **42** 1281–8
[7] Duchateau J, Turck B and Ciazynski D 1998 Coupling current losses in composites and cables: analytical calculations *Handbook of Applied Superconductivity* ed Seeber Bernd vol 2 (Taylor & Francis) pp 205–31
[8] Duchateau J, Turck B, Lacroix B, Schwarz M, Torre A and Zani L 2012 Stability of a cable in conduit conductor under fast magnetic field variations *IEEE Trans. Appl. Supercond.* **22** (3
[9] Bottura L and Marinucci M http://htess.com/cryosoft.htm Cryosoft
[10] Readman P 2014 *PFEU2 SULTAN Sample Test Report F4E_D_22TW6E* Fusion for Energy
[11] Bessette D 2016 *Assessment of the performance of the CSJA8 sample* ITER-IO
[12] van Lanen E P and Nijhuis A 2011 Simulation of interstrand coupling loss in cable-in-conduit conductors with JackPot-AC *IEEE Trans. Appl. Supercond.* **21** 1926–9

[13] Lanen E P, Nugteren J V and Nijhuis A 2012 Full-scale calculation of the coupling losses in ITER size cable-in-conduit conductors *Supercond. Sci. Technol.* **25** 8
[14] Reccia L *et al* 2010 Preparation of PF1/6 and PF2 conductor performance qualification sample *IEEE Trans. Appl. Supercond.* **21** 1930–3
[15] Stepanov B, Bruzzone P, Wesche R, Martovetsky N, Hatfield D, Vostner A and Devred A 2010 Impact of sample preparation procedure on the test results of four US ITER TF conductors *IEEE Trans. Appl. Supercond.* **20** 508–11
[16] Bruzzone P, Anchel A, Fuchs A, Pasztor G, Stepanov B, Vogel M and Vecsey G 2002 Upgrade of operating range for SULTAN test facility *IEEE Trans. Appl. Supercond.* **12** 520–3
[17] Breschi M *et al* 2012 Results of the TF conductor performance qualification samples for the ITER project *Supercond. Sci. Technol.* **25** 095004
[18] Breschi M, Carati D, Bessette D, Devred A, Romano G, Vostner A and Zhou C 2015 Performance analysis of the Nb–Ti conductor qualification samples for the ITER project *Supercond. Sci. Technol.* **28** 115001
[19] Bruzzone P, Fuchs A, Stepanov B and Vecsey G 2002 Transient stability results for Nb3Sn cable-in-conduit conductors *IEEE Trans. Appl. Supercond.* **12** 512–5
[20] Bottura L 2000 A practical fit for the critical surface of NbTi *IEEE Trans. Appl. Supercond.* **10** 1054–7
[21] Bottura L and Bordini B 2009 Jc(B, T) Parametrization for the ITER Nb3Sn production *IEEE Trans. Appl. Supercond.* **19** 1521–4
[22] Breschi M, Bessette D and Devred A 2011 Evaluation of effective strain and *n*-value of ITER TF conductor sample *IEEE Trans. Appl. Supercond.* **21** 1969–73
[23] Bottura L 2013 Cable stability *Proc. CERN Accelerator School*
[24] Bagnasco M 2009 Calorimetric method for current sharing temperature measurements in ITER conductor samples in SULTAN *Fusion Eng. Des.* **84** 423–6
[25] Breschi M, Trevisani L, Bottura L, Devred A and Trillaud F 2009 Comparing the thermal stability of NbTi and Nb3Sn wires *Supercond. Sci. Technol.* **22** 025019